Ultrasonics 97 (2019) 19–28

Contents lists available at ScienceDirect

Ultrasonics

journal homepage: www.elsevier.com/locate/ultras

Scratching-induced surface characteristics and material removal mechanisms in rotary ultrasonic surface machining of CFRP

Hui Wang[a], Fuda Ning[b], Yuanchen Li[a,c], Yingbin Hu[a], Weilong Cong[a,*]

[a] Department of Industrial, Manufacturing, and Systems Engineering, Texas Tech University, Lubbock, TX 79409, USA
[b] Department of Systems Science and Industrial Engineering, State University of New York at Binghamton, Binghamton, NY 13902, USA
[c] Key Laboratory of Mechanism Theory and Equipment Design of Ministry of Education, Tianjin University, Tianjin 300072, PR China

ARTICLE INFO

Keywords:
Rotary ultrasonic surface machining
CFRP
Material removal mechanism
Morphology
Cutting force

ABSTRACT

Rotary ultrasonic machining has been successfully explored in surface machining of carbon fiber reinforced plastic (CFRP) composites. It has been proven to be an effective and efficient CFRP machining method. Both theoretical and experimental investigations have been conducted with the assumption that the CFRP is removed by brittle fracture removal mode. However, in brittle material machining, ductile flow phenomenon still exists. Ductile scratching marks are also observed on the machined CFRP surfaces. It is still unknown that what actual material removal modes are under different machining variables. To investigate the material removal mechanisms in rotary ultrasonic surface machining (RUSM) of CFRP, single abrasive scratching tests were conducted. The scratching induced characteristics and scratching forces were analyzed. Both the ductile removal mode and the brittle fracture removal mode were observed and identified in both carbon fiber layers and epoxy resin layers on the machined marks by using scanning electron microscopy (SEM) imaging. With the increase of scratching depth, the material removal mode of CFRP was changed from the ductile removal mode to the brittle fracture mode. From the analysis of kinematic trajectory of diamond grain, the scratching cutting forces were decreased in the tests with the assistance of ultrasonic vibration under the same machining variables. The generation mechanisms of the delamination were analyzed and discussed.

1. Introduction

Rotary ultrasonic surface machining (RUSM), a non-traditional machining process, combines material removal from ultrasonic machining and traditional grinding, as shown in Fig. 1. In RUSM, the grinding tool with metal-bonded abrasive grains vibrates in axial direction at an ultrasonic frequency (typically 20 kHz) during machining. The workpiece feeds along the horizontal direction. The motion of abrasive grains on the tool consists of the rotation of the spindle, the feeding motion, and the ultrasonic vibration.

It was reported that RUSM had been successfully explored in surface machining of carbon fiber reinforced plastic (CFRP) composites, and it had been proven to be an effective and efficient machining method [1]. Both experimental and theoretical investigations had been reported. Wang et al. investigated the effects of tool variables in such a process. They found that smaller feeding-directional cutting forces were generated by using the tool with larger abrasive size, smaller abrasive concentration, two slots, or the convex geometry, and the lower surface roughness were produced by using the tool with smaller abrasive size, smaller abrasive concentration, two slots, or the convex geometry [2]. The effects of machining variables (including ultrasonic power, tool rotation speed, feedrate, and depth of cut) were studied in such a process. It was reported that both cutting forces (feeding-directional cutting force and axial-directional cutting force) and surface roughness could be decreased by using higher tool rotation speed, lower feedrate, or lower depth of cut, while using higher level of ultrasonic power led to lower cutting forces and higher surface roughness. The characteristics of machined surface morphology of CFRPs in RUM surface machining processes were also analyzed [3–5]. Wang et al. investigated effects of workpiece machining orientations in such a process, and they arrived at a conclusion that lower cutting forces (both feeding-directional cutting force and axial-directional cutting force) were produced by using 90° workpiece machining orientation, while lower surface roughness was generated by using 0° workpiece machining orientation [6]. Li et al. investigated effects of surface grinding methods (down grinding and up grinding) on cutting forces as well as surface quality in RUSM of CFRP composites. The results showed that compared with RUSM with down grinding method, RUSM with up grinding method

* Corresponding author.
E-mail address: weilong.cong@ttu.edu (W. Cong).

https://doi.org/10.1016/j.ultras.2019.04.004
Received 18 June 2018; Received in revised form 14 February 2019; Accepted 16 April 2019
Available online 17 April 2019
0041-624X/

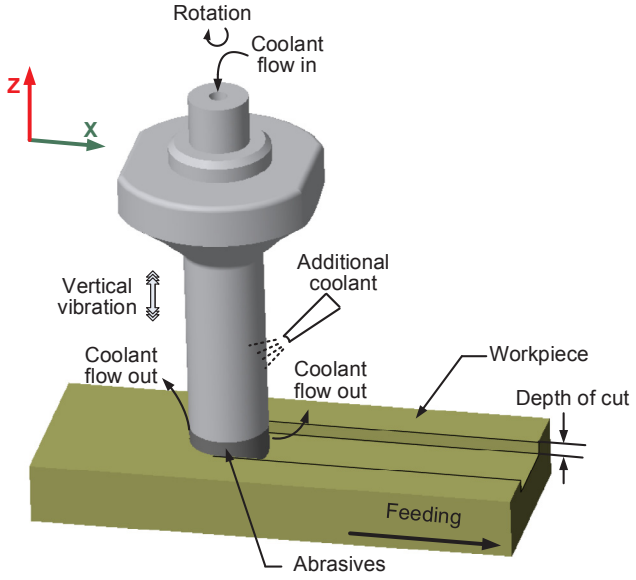

Fig. 1. Illustration on rotary ultrasonic surface machining (RUSM).

produced longer total cutting path, larger fiber fracture size, and larger resin chip size, thus leading to higher cutting force and higher surface roughness [7]. Geng et al. extended the rotary ultrasonic elliptical machining (RUEM) to surface machining of CFRP and found that RUEM surface machining of CFRP produced the decreased cutting force, an extended tool life, and the improved surface quality owing to the excellent chip removal conditions and intermittent material removal mechanisms in RUEM [8]. Geng et al. investigated the effects of speed ratio (the ratio between the nominal cutting speed and the maximum speed of tool vibration in cutting direction) on cutting forces, surface quality, and tool wear in RUEM surface machining of CFRP. It was reported that lower speed ratio was preferable to the lower cutting forces, less surface defects, and lower tool wear due to the lower tool-workpiece contacting ratio [9]. The decrease of cutting force was mainly due to the generated extra additional speed in the cutting direction and the greatly lowered contact friction between the tool and workpiece [10]. Ning et al. built the theoretical model to investigate the relationships between the feeding-directional cutting force and input variables in RUSM of CFRPs. It was shown that the feeding-directional cutting force decreased as abrasive concentration, depth of cut, and feedrate decreased, or as ultrasonic vibration amplitude, tool rotation speed, and abrasive size increased [11]. Based on the brittle fracture mechanism, Liu et al. investigated the relationships between the cutting force in axial direction and input variables by developing a theoretical model in RUSM of CFRPs. They argued that the cutting force in axial direction decreased as the increase of tool rotation speed, or as the decrease of feedrate and depth of cut [12]. In those investigations, CFRP was treated as a brittle material. However, Pei et al. reported that ductile flow phenomenon still existed in brittle material machining [13]. Zhang et al. found that ductile scratching marks were also observed on the machined surface of other brittle materials [14]. It is still unknown that what actual material removal modes are in RUSM of CFRP under different machining variables. In addition, the reported investigations focused on the material removal modes by optimizing the machining variables or simulating the machining processes. It will be of great help to investigate the actual material removal modes to study the RUSM processes of CFRP composites from microscopic perspectives.

There were no reported investigations on evaluating material removal mechanisms in RUSM of CFRP composites, especially for the cutting of carbon fiber layers and epoxy resin layers in CFRPs, respectively. To evaluate the material removal mechanisms in RUSM, the single abrasive scratching test was applied. Such a test could also be used to evaluate the surface scratching resistance and tribology properties of the workpiece. Zhang et al. suggested that the material removal modes would be determined by analyzing deformation modes, which were obtained from the surface morphology generated by the scratching test [14].

CFRP composites were regarded as difficult-to-cut materials due to CFRP's properties of inhomogeneity and anisotropy as well as the carbon fibers' high abrasive resistance [15]. The material removal modes might be different under the different machining conditions when scratching CFRP composites. In surface machining processes of CFRPs, carbon fiber layers and matrix layers are usually cut alternatively. Due to this reason, cutting carbon fiber layers and matrix layers by turns is a better choice to investigate the material removal mechanisms from microscopic directions in surface machining of CFRPs.

The single abrasive scratching tests will be conducted under different levels of ultrasonic vibration to investigate the material removal mechanisms in RUSM of CFRPs. The scratching-induced surface characteristics will be analyzed. The analysis of surface morphology in both carbon fiber layers and matrix layers of CFRPs will be conducted to investigate the real material removal mechanisms. The scratching forces will also be discussed to investigate the material removal mechanisms in RUSM of CFRP composites. In addition, the difference between the kinematic trajectory of abrasive grain with and without ultrasonic vibration will be also analyzed. The generation mechanisms of the delamination and the deformation features of scratching exit will be discussed.

2. Workpiece properties, experiment set-up and conditions, and measurement procedures

2.1. Workpiece properties

The CFRP composite workpiece, used in the scratching test, had the dimension of 40 mm × 18.5 mm × 18 mm. Table 1 shows the CFRP properties. The side edge of CFRP was used to conduct scratching tests. The CFRP workpiece had 23 layers of carbon fibers on the side edges. The volume fractions of carbon fibers and epoxy resin in CFRP were 67% and 33%, respectively. Before the scratching tests, the selected edge of the CFRP workpiece was polished to achieve a good starting surface quality with the surface roughness of 0.4 μm. The scratching direction was perpendicular to carbon fiber layers, and the diamond indenter, being shown in Fig. 2, cut carbon fiber layers and the epoxy matrix layers alternatively. This diamond indenter had the point angle of 100°.

2.2. Experiment set-up and conditions

The scratching test was conducted on a rotary ultrasonic machine (Series 10, Sonic-Mill, Albuquerque, New Mexico, USA). Fig. 2 shows

Table 1
Workpiece properties.

Property	Unit	Value
Density of CFRP	kg/m^3	1600
Hardness (Rockwell)	HRB	67–73
Density (carbon fibers)	kg/m^3	1800
Elastic modulus (carbon fibers)	GPa	230
Tensile strength (carbon fibers)	GPa	5
Poisson's ration (carbon fibers)	–	0.3
Fracture toughness (carbon fibers) (Energy/G_c)	J/m^2	2
Density (epoxy matrix)	kg/m^3	1200
Elastic modulus (epoxy matrix)	GPa	4.5
Tensile strength (epoxy matrix)	MPa	130
Poisson's ration (epoxy matrix)	–	0.4
Fracture toughness (epoxy matrix) (Energy/G_c)	J/m^2	500

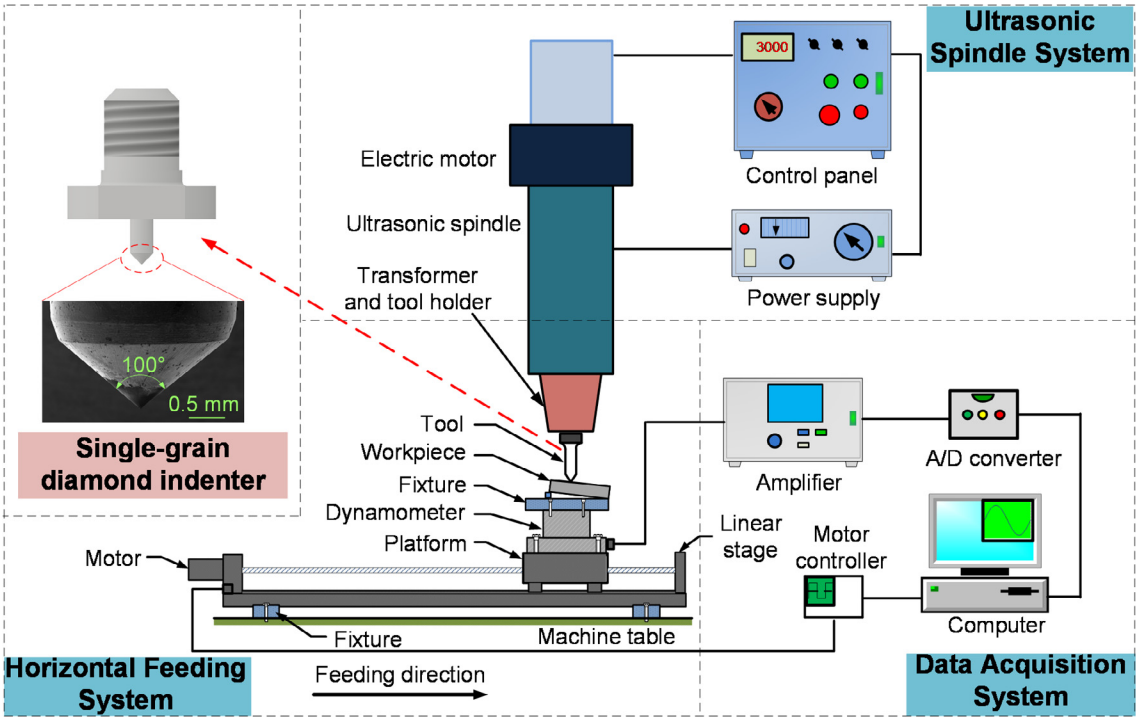

Fig. 2. Illustrations on RUSM experimental setup.

that this experimental setup consists of an ultrasonic spindle system, a horizontal feeding system, and a data acquisition system. The ultrasonic spindle system was used to generate ultrasonic vibration with high frequency (typically 20 kHz) and transmit this ultrasonic vibration to the diamond indenter for scratching tests. The horizontal feeding system provided the feeding motion for the scratching tests of CFRP composites. This feeding system included a linear stage (D-slide 400 mm, Newmark, Rancho Santa Margarita, California, USA), a motion controller (NSC-A1, Newmark), and a software (QuickMotion NSC-A1, Newmark). Both the dynamometer and the CFRP workpiece were fixed on the platform of the linear stage. The data acquisition system (DAQ) was used to collect the data of cutting forces. More detail information of DAQ will be given in the section of measurement procedures.

Fig. 3 shows the illustration on scratching test set-up. The insert gauge was used to generate an elevation angle of 0.3° for the CFRP workpiece. Due to this inclining angle, the depth of the scratching test was increased from zero to the final depth. The diamond indenter with the 100° point angle was applied, and its motion in the scratching test was a combination of horizontal feeding motion (along the X-axis of the machine) and ultrasonic vibration. Fig. 4 shows the kinematic characteristics of the diamond indenter in a cycle time of ultrasonic vibration. The vibration amplitudes for the ultrasonic power of 0%, 40%, and 80% were 0 μm, 3 μm, and 5 μm, respectively. The scratching velocity in horizontal direction was 100 mm/s.

2.3. Measurement procedures

A Kistler dynamometer (Type 9272, Kistler Inc., Winterthur, Switzerland) was used to measure the scratching generated forces in horizontal feeding and normal directions. The electrical analogy signals from the dynamometer were transmitted to a charge amplifier (Type 5070, Kistler Inc.). Through amplifier, the amplified analogy signals were then transformed into digital signals by an A/D converter (Type 5697A, Kistler Inc.). A computer then recorded these digital signals with the help of a DynoWare software (Type 2825 D-02, Kistler Inc.). In this investigation, the sampling frequency was set at 20 kHz to obtain more data. After obtaining the data, they were diluted 20 times to

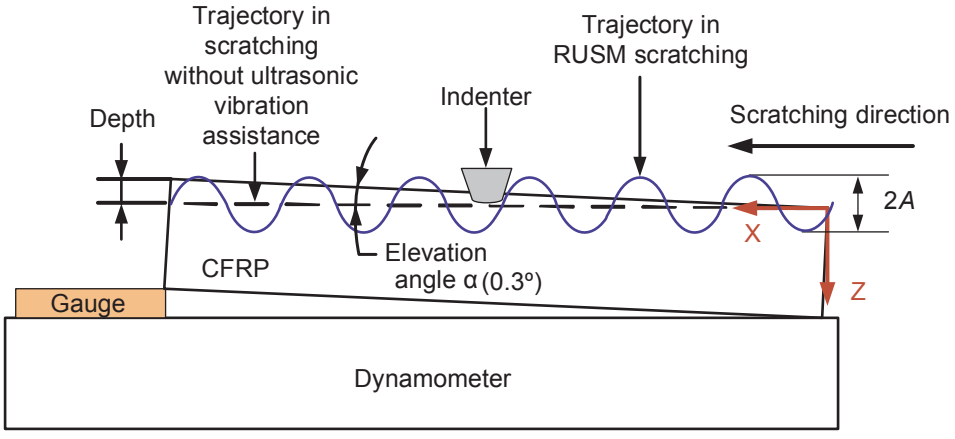

Fig. 3. Illustrations on scratching test set-up.

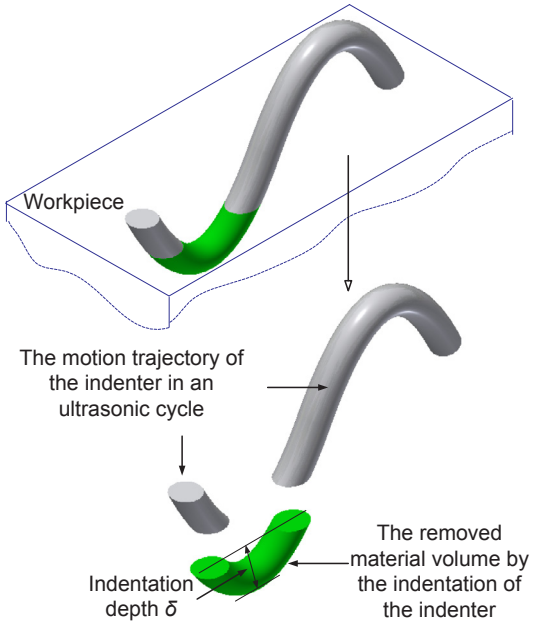

Fig. 4. The kinematic characteristics of the diamond indenter in a cycle time of ultrasonic vibration.

achieve the average cutting force, which were shown in cutting force curve. The averaged cutting force was then used to evaluate the cutting process instead of the dynamic cutting force in each ultrasonic vibration cycle time [16]. Scanning electron microscopies (SEM) (Crossbeam 540, Carl Zeiss AG, Oberkochen, Germany and S-4300, Hitachi Co., Tokyo, Japan) were used to observe the microscopic deformation characteristics of the machined surface and the microstructure characteristics of scratching grooves under different levels of ultrasonic power. By analyzing these surface characteristics, the actual material removal mechanisms can be obtained.

3. Experimental results

3.1. Scratching-induced characteristics and material removal modes

Two kinds of material removal modes in CFRP can be observed in Fig. 5. Bifano et al. reported that the ductile material removal mode occurred when the scratching depth was smaller than the critical depth [17]. Wang et al. argued that this mode included elastic mode and plastic mode. In elastic mode, no chip was formed, and the elastic deformation was the predominant deformation mode [18]. In plastic mode, the undeformed chip thickness was smaller than the critical depth. Moreover, in ductile material removal mode, the lateral cracking did not exist and the simple plastic flow was the favored deformation form. In ideal ductile removal mode, the surface can approach zero damage, and it can be machined without fracture-induced damage, such as the cracking. The abrasive penetration volume should be equal to the material removal volume. Fig. 5b shows the brittle material removal mode. As the scratching depth exceeded the critical depth, the fracture occurred in the machined zone's surface and subsurface. Wang et al. argued that in brittle fracture removal mode, the material was removed with the cracks' formation and propagation to the workpiece

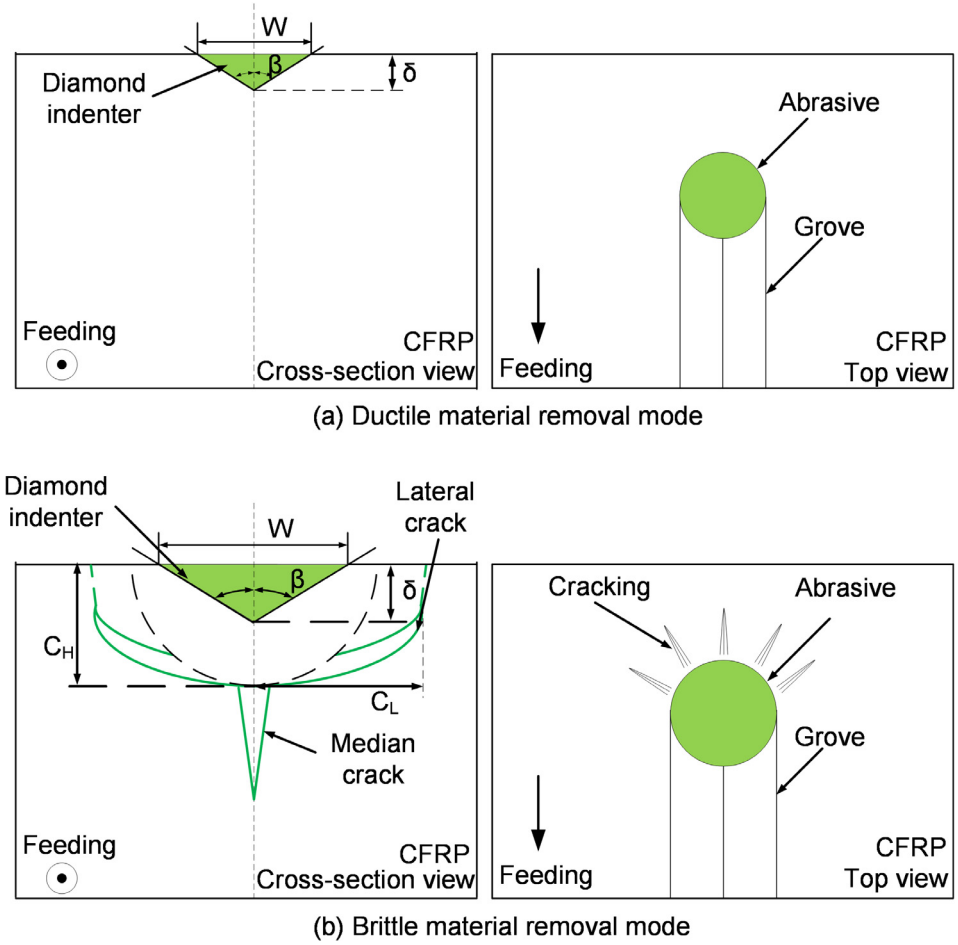

Fig. 5. Illustrations on material removal modes.

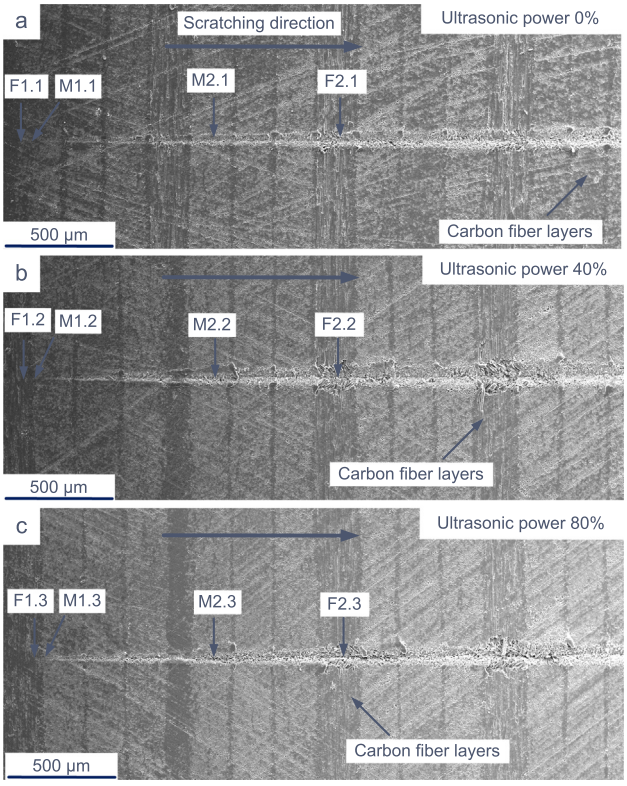

Fig. 6. Overall SEM images of the scratching test morphology with different levels of ultrasonic power (F1: ductile removal mode in carbon fiber layers; M1: ductile removal mode in matrix layers; F2: brittle removal mode in carbon fiber layers; M2: brittle removal mode in matrix layers).

surfaces. The material removal volume should be much larger than abrasive penetration volume [19].

Fig. 6 shows the overall SEM images of the scratching test morphology with different levels of ultrasonic power. Two typical deformation regions in both carbon fiber layers (F1 and F2) and epoxy resin layers (M1 and M2) in each scratching test were selected to investigate the scratching-induced characteristics, material removal features, and material removal modes. F1 and M1 are selected to illustrate the ductile removal mode in carbon fiber layers and matrix layers, respectively. F2 and M2 are typical examples to illustrate the brittle fracture removal mode in carbon fiber layers and matrix layers, respectively. The scratching depths for these above regions (F1, M1, M2, and F2) are 80 nm, 120 nm, 4.6 μm, and 8.1 μm, respectively.

3.1.1. Ductile removal mode phenomena

The comparisons on the characteristics of carbon fiber layers in ductile removal mode at the scratching depth of 80 nm under three different levels of ultrasonic power are shown in Fig. 7. When scratching depth is low, a smaller amount of materials is removed from the top section of carbon fibers. It can be seen that no cracking and fracture-induced damages could be observed on the machined surface. The smooth morphologies of carbon fiber layers show that the ductile removal mode should dominate the material removal in this region. The differences among these three tests in these regions are not clear.

Fig. 8 illustrates the comparisons on characteristics of epoxy resin layers in ductile removal mode at the scratching depth of 120 nm. Both the fracture-induced damage and the cracking are not shown on the machined surfaces in Fig. 8. The scratching-induced characteristics of the morphology show that the major material removal mode should belong to ductile removal mode. In the ultrasonic vibration-assisted (UVA) scratching tests, the high-frequency vibration of the single diamond indenter caused the ultrasonic impact action, leading to the

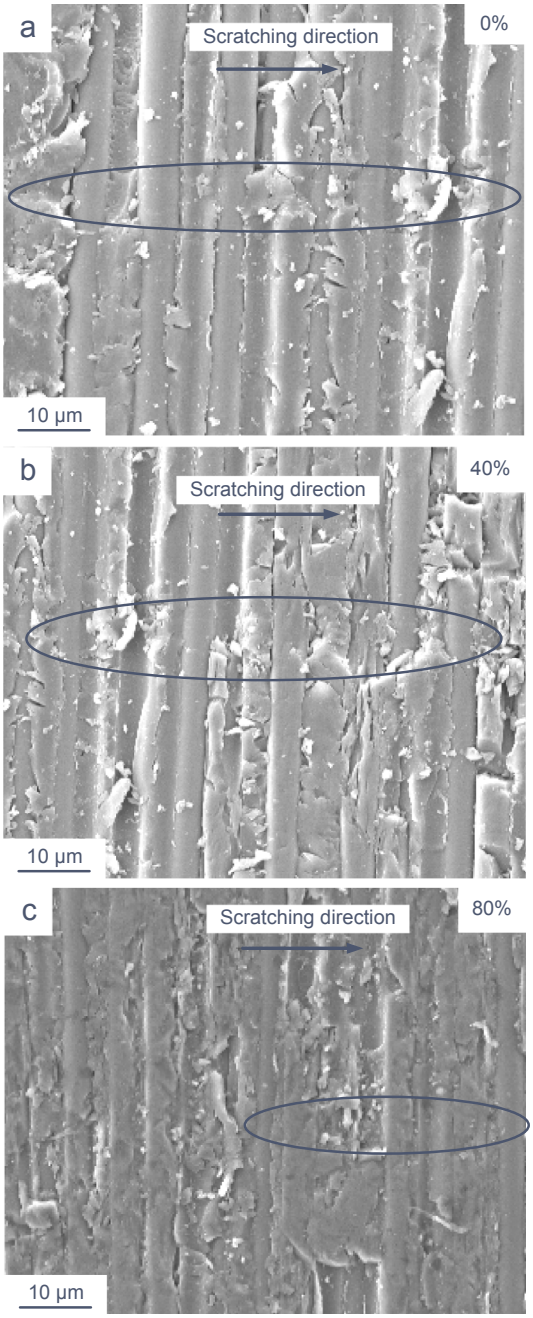

Fig. 7. The comparisons on the characteristics of carbon fiber layers in ductile removal mode at the scratching depth of 80 nm under three different levels of ultrasonic power.

discontinuous scratching processes. Moreover, the UVA scratching tests (both the test under ultrasonic power of 40% and that under ultrasonic power of 80%) showed the ultrasonic trajectory trace induced by ultrasonic vibration. The distance (5 μm) between two neighboring trajectory trace in UVA scratching tests was the traveling distance of the single diamond indenter in one cycle time of ultrasonic vibration.

3.1.2. Brittle fracture removal mode phenomena

Fig. 9 shows the comparisons on characteristics of carbon fiber layers in brittle fracture mode at the scratching depth of 8.1 μm. A clear groove in the section of carbon fiber layers was produced. At the groove edges, the scratching-induced characteristics, including removed carbon fibers, voids, brittle fracture, fiber pullout, etc., were generated in these regions. Besides, Wang et al. reported that the tearing, denoting

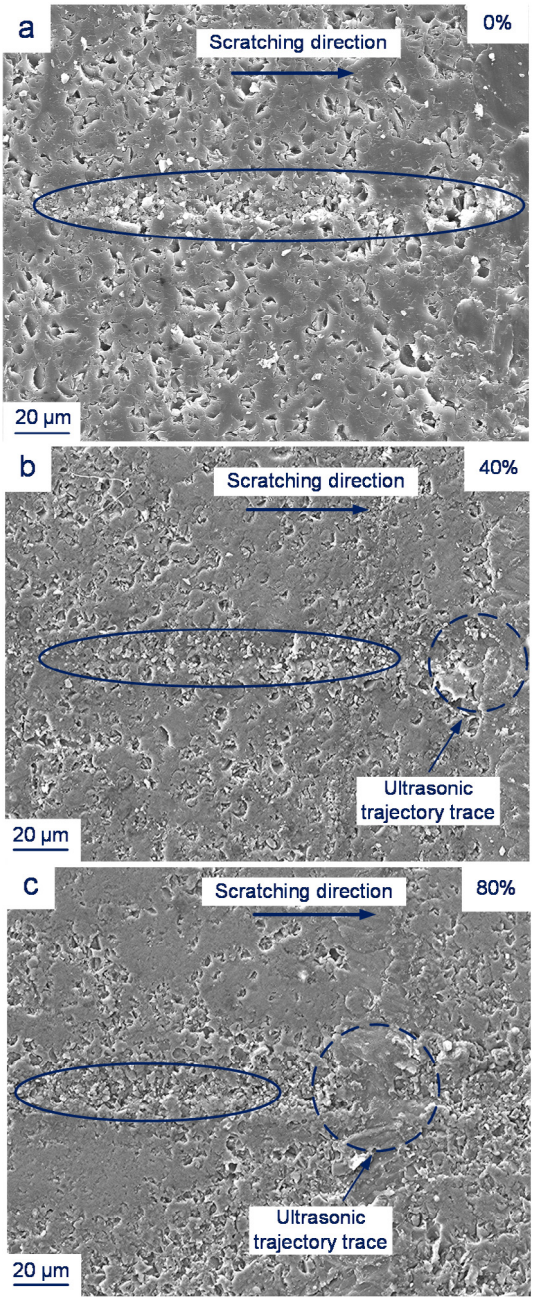

Fig. 8. The comparisons on characteristics of epoxy resin layers in ductile removal mode at the scratching depth of 120 nm.

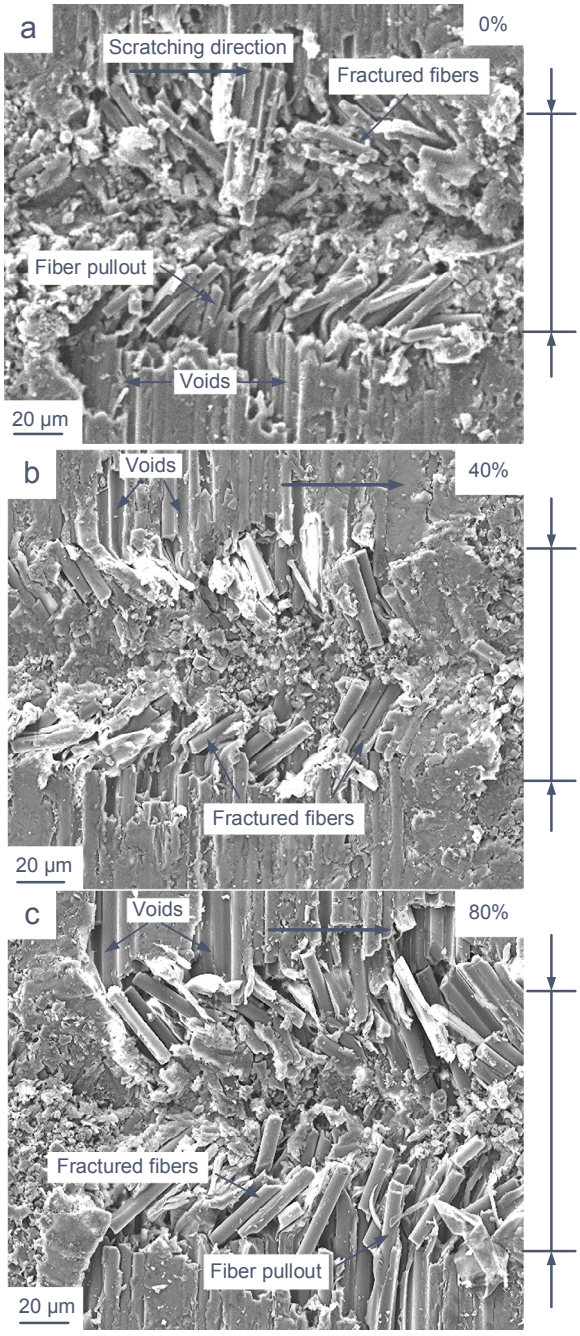

Fig. 9. The comparisons on characteristics of carbon fiber layers in brittle fracture mode at the scratching depth of 8.1 μm.

fiber fracture and exposing other fibers under them, was also one of the characteristics of brittle fracture removal mode [20]. Compared with the test without ultrasonic vibration in Fig. 9a, the UVA scratching tests of CFRPs in Fig. 9b and c showed obviously different deformation features. The grooves' widths in UVA scratching tests were larger due to the up-and-down ultrasonic vibration of the diamond indenter with a point angle of 100°. The lateral cracks, induced by ultrasonic vibration in UVA scratching tests, caused the fractured carbon fibers along both edges of scratching grooves.

Fig. 10 shows the comparisons on the characteristics of epoxy resin layers in brittle fracture mode at the scratching depth of 4.6 μm under three different levels of ultrasonic power. It can be seen that each scratching test shows a clear groove. At both edges of these grooves, tearing regions (denoting matrix fracture and exposing other matrix regions under it) and chipping dents were produced. The interaction and propagation among lateral cracks could result in these tearing regions and chipping dents at the groove edges. This case was consistent with the phenomena reported by Wang et al. [21]. Fig. 10b and c show the ultrasonic trajectory trace with the distance of 5 μm between two neighboring trajectory trace, which was generated from sinusoidal motion of diamond indenter due to the multiple cutting cycles of ultrasonic vibration. The scratching widths of the grooves in UVA scratching tests were larger than those without ultrasonic vibration. The wider scratching grooves in UVA scratching tests were due to the indenter tip structure with a certain angle of 100°. This case led to a better machining performance in the UVA scratching tests of CFRPs, compared to the scratching test without ultrasonic vibration. Moreover, the actual scratching depths in scratching tests were less than the expected depths due to the counteraction of CFRPs and synergy between

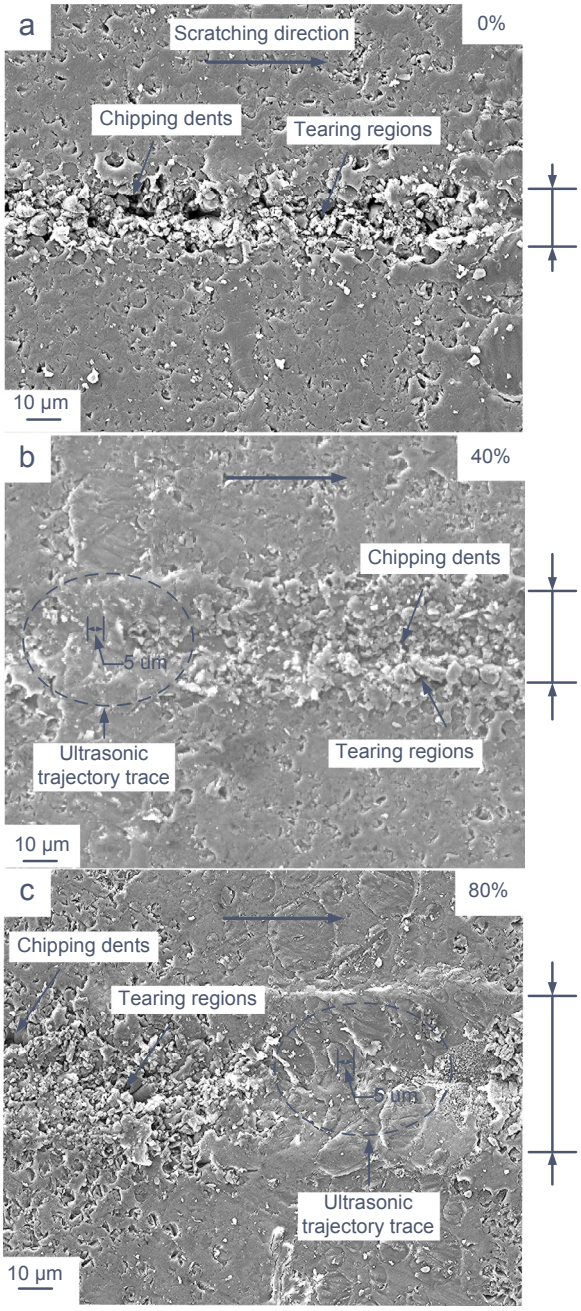

Fig. 10. The comparisons on characteristics of epoxy resin layers in brittle fracture mode at the scratching depth of 4.6 μm.

carbon fibers and epoxy resin.

3.2. Scratching forces

3.2.1. Scratching forces and material removal modes

The scratching forces (feeding-directional force) in feeding direction are shown in Fig. 11. It can be seen that the curve of these forces mainly consisted of the force signals with different levels of fluctuations. Arif et al. reported that based on the plasticity theory, with the increase of depth of cut, the scratching forces increased with smaller fluctuations during the cutting process under ductile removal mode [22]. In this investigation, the scratching range with ductile removal mode was very short. All the feeding-directional forces in these areas had smaller variances. After a certain depth, being called as the critical depth by Zhang et al. [23], the force signals abruptly increased with significant

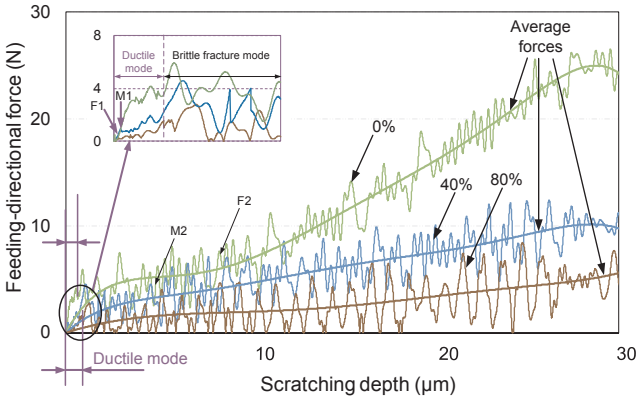

Fig. 11. The comparisons on feeding-directional forces.

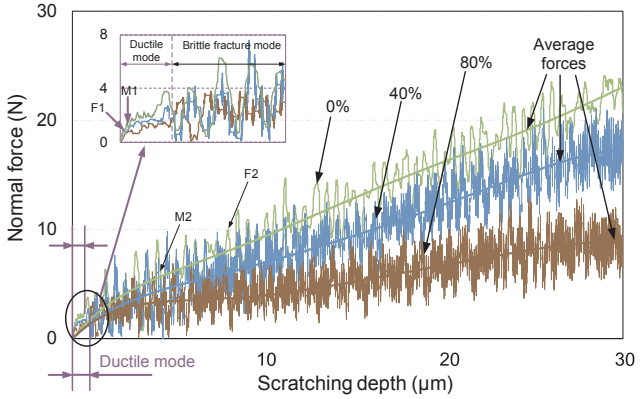

Fig. 12. The comparisons on normal forces.

fluctuations, which meant that the material removal mode in those stages of scratching tests was brittle fracture mode.

Compared with the scratching tests without ultrasonic vibration, UVA scratching tests of CFRPs generated lower average feeding-directional force and longer track with ductile removal mode. The first major reason for the reduction of feeding-directional force in UVA scratching tests was that the trajectory length of the diamond indenter in UVA scratching tests was longer than without ultrasonic vibration [24], as shown in Fig. 4. The second reason was that the intermittent contact, the smaller chips, and the periodically changed scratching velocity, being generated from the ultrasonic vibration [25], resulted in the smaller friction force between the diamond indenter and the workpiece, leading to the smaller feeding-directional force in UVA scratching tests.

Fig. 12 shows the comparisons of normal forces among scratching tests under different levels of ultrasonic power. With the increase of scratching depth, the normal forces were increased in all three scratching tests. When the scratching depth was smaller than critical depth, the cutting processes showed ductile removal mode. With this case, the normal forces increased with smaller fluctuation under all three different levels of ultrasonic vibration. After the critical depth, the normal forces had much larger fluctuation, indicating that the material removal mode was brittle removal mode.

Compared with the average normal force in scratching tests without ultrasonic vibration, the average normal forces generated in UVA scratching tests of CFRPs were lower. With the increase of ultrasonic power, the average normal force was decreased. Moreover, UVA scratching tests generated normal forces with the changing trends of ultrasonic vibration, which were also not shown in the feeding-directional forces in UVA scratching tests. This phenomenon showed that the ultrasonic vibration induced much direct effects on normal forces. The major reason for the reduction of normal force in UVA scratching tests

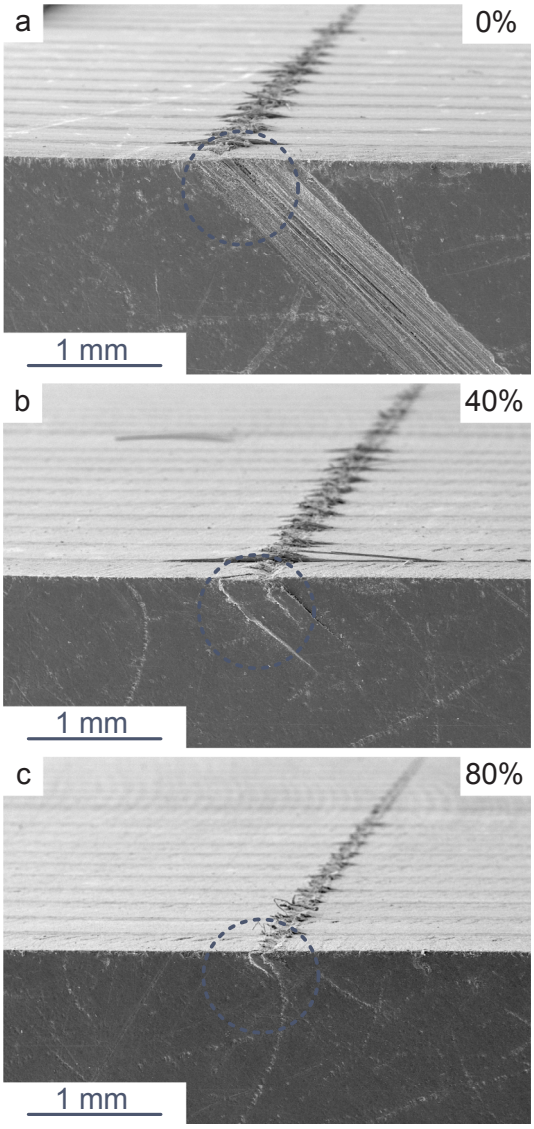

Fig. 13. The comparisons on the delamination on the exit side.

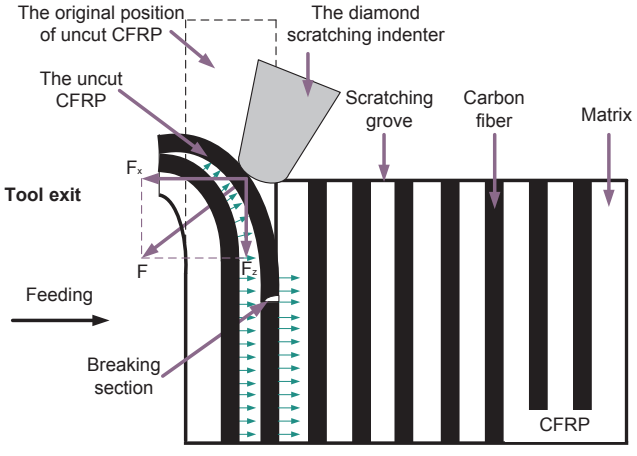

Fig. 14. The illustration on the generation of delamination at the tool exit.

was discussed as follows. Wang et al. reported that there were no causal relationships between material removal rate and ultrasonic vibration amplitude, indicating that material removal rate was not determined by the ultrasonic vibration amplitude [26]. To keep the removed material volume unchanged, the grain indentation depth would be decreased with the increase of ultrasonic vibration amplitude, leading to the decrease of normal force. Other reasons for the reduction of normal forces will be discussed by analyzing the kinematic trajectory of diamond indenter in the next section.

3.2.2. Effects of ultrasonic power on scratching forces

The motion of a single abrasive grain was composed of workpiece feedrate and ultrasonic vibration in the direction of the Z axis. Based on this motion analysis, the kinematic trajectory model of a single abrasive grain can be obtained by Eq. (1).

$$\begin{cases} x = f_r t \\ z = A\sin(2\pi f t) \end{cases} \tag{1}$$

where f_r is the feedrate of workpiece, mm/s; t is the processing time, s; A is the amplitude of ultrasonic vibration, mm; f is the frequency of ultrasonic vibration, Hz.

The velocity of a single abrasive grain can be achieved by Eq. (2).

$$\begin{cases} v_x = f_r \\ v_z = 2\pi f A\cos(2\pi f t) \end{cases} \tag{2}$$

The trajectory length L of a single abrasive grain in a single cycle time (T) of ultrasonic vibration can be expressed by following Eqs. (3) and (4).

$$L = \int_0^T (\sqrt{v_x^2 + v_z^2})dt \tag{3}$$

$$L = \int_0^{\frac{1}{f}} (\sqrt{f_r^2 + (2\pi f A\cos(2\pi f t))^2})dt \tag{4}$$

The average velocity of the diamond indenter can be described as

$$\bar{V} = \frac{L}{T} = \frac{\int_0^{\frac{1}{f}} (\sqrt{f_r^2 + (2\pi f A\cos(2\pi f t))^2})dt}{T} \tag{5}$$

Based on Eq. (4), the trajectory length of scratching diamond indenter in the UVA scratching test was longer than that without ultrasonic vibration within the same time interval. By Eq. (5), the average velocity of the diamond indenter was higher in UVA scratching tests than that without ultrasonic vibration under the same processing conditions. The higher average velocity resulted in the smaller simultaneous cutting volume under the same *MRR*. This case resulted in the decreased scratching forces in UVA scratching tests. With the increase of ultrasonic power, the amplitude of ultrasonic vibration was increased. The kinematic trajectory length of diamond indenter was increased. To keep the material removal rate *MRR* unchanged, the scratching depth was then decreased. Matsumura et al. found that in surface machining of brittle materials with the diamond tool, the decrease of depth of cut caused the decrease of cutting force at the cutting depth below 100 μm [27]. For the same material removal rate, the simultaneous cutting volume in UVA scratching tests was also smaller than that without ultrasonic vibration, due to the higher average velocity in UVA scratching tests. The smaller simultaneous cutting volume resulted in smaller indentation depth. For the normal force, it was mainly affected by the indentation depth, and it had the positive relationships with the indentation depth. This was the reason why the curve of normal force showed the trends of ultrasonic vibration.

3.3. The comparisons on delamination

The effects of ultrasonic power on delamination in the exit sections of scratching tests are shown in Fig. 13. In scratching tests without ultrasonic vibration, the area with the push-out materials at the exiting section was the largest, generating the heaviest delamination. Compared with the scratching tests without ultrasonic vibration, the scratching test with the ultrasonic power of 40% generated smaller

delamination, while that with the ultrasonic power of 80% produced the smallest delamination. The major reason for the reduction of delamination in UVA scratching tests was that the scratching forces in UVA scratching tests were smaller than those without ultrasonic vibration.

Fig. 14 illustrates the generation model of delamination at the tool exit. The feeding-directional force and the normal force were generated when the diamond indenter was cutting the uncut CFRP material. Jia et al. reported that the uncut carbon fibers of CFRP were squeezed and pushed towards the tool exit with weak back support, since the bonding strength between carbon fibers and matrix was much lower than transverse compressive strength, the transverse shear strength, or the longitudinal tensile strength [28]. The reason was that in the transverse direction of CFRPs, the bonding force and the support of last few carbon fibers were weak, and they determined the constraints of the uncut CFRP material. As a result, the bonding between carbon fibers and matrix was forced to reach the ultimate strength value before carbon fibers were broken, leading to the debonding between carbon fibers and matrix. Hintze and Hartmann found that for carbon fibers, the attainment of tension stress of carbon fibers or transverse rupture strain or stress resulted in the breakage of carbon fibers [29]. At the tool exit, the cutting motion of diamond indenter also caused the deflection of debonded carbon fibers, which decreased the transverse cutting stress at the interface between the tool and the workpiece. Jia et al. found that this case could lead to carbon fibers' small fracture. The deflection of carbon fibers also caused the concentration of stress under the scratching groves, leading to the bending fracture of carbon fibers [30]. Moreover, the matrix in the uncut CFRP could be fractured into small debris, leading to the debonding of carbon fibers in the uncut CFRP and then the decreased modulus of the uncut CFRP. Such debonding carbon fibers could not cause the rupture of carbon fibers, which were pressed under the scratching indenter without being cut after the passing of the indenter. Due to the above analysis, the delamination was formed at the tool exit.

4. Conclusions

By conducting the scratching tests, the material removal mechanisms were explored, and scratching-induced characteristics and the scratching forces (feeding-directional forces and normal forces) were analyzed and discussed. The conclusion can be drawn as follows.

(1) Both carbon fiber layers and epoxy resin matrix layers showed the ductile removal mode at very low scratching depth and brittle removal mode when scratching depth was larger. In the ductile removal mode, the surface was machined without fracture-induced damages, such as the cracking, while in the brittle fracture removal mode, the material was removed with the cracks' formation and propagation to the workpiece surfaces and the material removal performance was improved.
(2) The scratching forces (both the feeding-directional force and the normal force) in all scratching tests increased with the increase of scratching depth. When the scratching depth was smaller, the scratching forces had smaller fluctuation, indicating the material removal mode was ductile removal mode. When the scratching depth was larger than critical depth, the scratching forces had significant fluctuation, showing the characteristics of brittle fracture removal mode. Compared with the scratching tests without ultrasonic vibration, UVA scratching tests generated normal forces with the changing trends of ultrasonic vibration, which were also not shown in the feeding-directional forces in UVA scratching tests.
(3) The characteristics of scratching grooves in UVA scratching tests were generated by the combined effects of feeding motion and ultrasonic vibration. These characteristics included grooves, voids, fiber pullout, fractured fibers, waves induced by ultrasonic vibration, etc. By analyzing the generation mechanisms of the delamination and the deformation features of scratching exit, the delamination could be decreased with the increase of ultrasonic power.

Acknowledgment

The work was supported by U.S. National Science Foundation through award CMMI-1538381.

Declarations of interest

None.

References

[1] H. Wang, Y. Hu, F.D. Ning, Y.Z. Li, M. Zhang, W.L. Cong, S. Smallwood, Surface grinding of CFRP composites using rotary ultrasonic machining: effects of ultrasonic power, ASME 2017 6th International Conference on Materials and Processing, American Society of Mechanical Engineers, 2017, , https://doi.org/10.1115/MSEC2017-2726 pp. V001T02A045-V001T02A045.
[2] H. Wang, F.D. Ning, Y.B. Hu, P.K.S.C. Fernando, Z.J. Pei, W.L. Cong, Surface grinding of carbon fiber–reinforced plastic composites using rotary ultrasonic machining: effects of tool variables, Adv. Mech. Eng. 8 (9) (2016), https://doi.org/10.1177/1687814016670284 1687814016670284.
[3] H. Wang, W.L. Cong, F.D. Ning, Y.B. Hu, A study on the effects of machining variables in surface grinding of CFRP composites using rotary ultrasonic machining, Int. J. Adv. Manuf. Technol. 95 (9–12) (2018) 3651–3663, https://doi.org/10.1007/s00170-017-1468-6.
[4] F. Ning, H. Wang, Y. Hu, W. Cong, M. Zhang, Y. Li, Rotary ultrasonic surface machining of CFRP composites: a comparison with conventional surface grinding, Procedia Manuf. 10 (2017) 557–567, https://doi.org/10.1016/j.promfg.2017.07.049.
[5] H. Wang, F.D. Ning, Y.B. Hu, D.P. Du, W.L. Cong, Surface grinding of CFRP composites using rotary ultrasonic machining: design of experiment on cutting force, torque, and surface roughness, Int. J. Manuf. Res. 12 (4) (2017) 461–479, https://doi.org/10.1504/IJMR.2017.10008389.
[6] H. Wang, F.D. Ning, Y.B. Hu, W.L. Cong, Surface grinding of CFRP composites using rotary ultrasonic machining: a comparison of workpiece machining orientations, Int. J. Adv. Manuf. Technol. (2017), https://doi.org/10.1007/s00170-017-1401-z.
[7] Y.C. Li, C.Z. Ren, H. Wang, Y.B. Hu, F.D. Ning, X.L. Wang, W.L. Cong, Edge surface grinding of CFRP composites using rotary ultrasonic machining: comparison of two machining methods, Int. J. Adv. Manuf. Technol. 1–12 (2018), https://doi.org/10.1007/s00170-018-2901-1.
[8] D. Geng, D. Zhang, Y. Xu, F. He, D. Liu, Z. Duan, Rotary ultrasonic elliptical machining for side milling of CFRP: Tool performance and surface integrity, Ultrasonics 59 (2015) 128–137, https://doi.org/10.1016/j.ultras.2015.02.006.
[9] D. Geng, D. Zhang, Y. Xu, X. Jiang, Z. Lu, D. Lu, Effect of speed ratio in edge routing of carbon fiber-reinforced plastics by rotary ultrasonic elliptical machining, J. Reinf. Plast. Compos. 34 (21) (2015) 1779–1790, https://doi.org/10.1177/0731684415597483.
[10] Z. Li, D. Zhang, W. Qin, D. Geng, Feasibility study on the rotary ultrasonic elliptical machining for countersinking of carbon fiber–reinforced plastics, Proc. Inst. Mech. Eng., Part B: J. Eng. Manuf. 231 (13) (2017) 2347–2358, https://doi.org/10.1177/0954405415626086.
[11] F.D. Ning, W.L. Cong, H. Wang, Y.B. Hu, Z.L. Hu, Z.J. Pei, Surface grinding of CFRP composites with rotary ultrasonic machining: a mechanistic model on cutting force in the feed direction, Int. J. Adv. Manuf. Technol. 92 (1–4) (2017) 1217–1229, https://doi.org/10.1007/s00170-017-0149-9.
[12] S. Liu, T. Chen, C. Wu, Rotary ultrasonic face grinding of carbon fiber reinforced plastic (CFRP): a study on cutting force model, Int. J. Adv. Manuf. Technol. 89 (1–4) (2017) 847–856, https://doi.org/10.1007/s00170-016-9151-x.
[13] Z.J. Pei, P.M. Ferreira, M. Haselkorn, Plastic flow in rotary ultrasonic machining of ceramics, J. Mater. Process. Technol. 48 (1–4) (1995) 771–777, https://doi.org/10.1016/0924-0136(94)01720-L.
[14] C. Zhang, P. Feng, J. Zhang, Ultrasonic vibration-assisted scratch-induced characteristics of C-plane sapphire with a spherical indenter, Int. J. Mach. Tools Manuf 64 (2013) 38–48, https://doi.org/10.1016/j.ijmachtools.2012.07.009.
[15] H. Wang, F.D. Ning, Y.B. Hu, Y.C. Li, X.L. Wang, W.L. Cong, Edge trimming of carbon fiber-reinforced plastic composites using rotary ultrasonic machining: effects of tool orientations, Int. J. Adv. Manuf. Technol. 98 (5–8) (2018) 1641–1653, https://doi.org/10.1007/s00170-018-2355-5.
[16] D. Geng, Z. Lu, G. Yao, J. Liu, Z. Li, D. Zhang, Cutting temperature and resulting influence on machining performance in rotary ultrasonic elliptical machining of thick CFRP, Int. J. Mach. Tools Manuf 123 (2017) 160–170, https://doi.org/10.1016/j.ijmachtools.2017.08.008.
[17] T.G. Bifano, T.A. Dow, R.O. Scattergood, Ductile-regime grinding: a new technology for machining brittle materials, J. Eng. Indus. 113 (2) (1991) 184–189, https://doi.org/10.1115/1.2899676.
[18] S. Wang, C. An, F. Zhang, J. Wang, X. Lei, J. Zhang, An experimental and theoretical investigation on the brittle ductile transition and cutting force anisotropy in cutting KDP crystal, Int. J. Mach. Tools Manuf 106 (2016) 98–108, https://doi.org/10.

1016/j.ijmachtools.2016.04.009.
[19] J.J. Wang, C.L. Zhang, P.F. Feng, J.F. Zhang, A model for prediction of subsurface damage in rotary ultrasonic face milling of optical K9 glass, Int. J. Adv. Manuf. Technol. 83 (1–4) (2016) 347–355, https://doi.org/10.1007/s00170-015-7567-3.
[20] J.J. Wang, P.F. Feng, J.Z. Zheng, J.F. Zhang, Improving hole exit quality in rotary ultrasonic machining of ceramic matrix composites using a compound step-taper drill, Ceram. Int. 42 (12) (2016) 13387–13394, https://doi.org/10.1016/j.ceramint.2016.05.095.
[21] J.J. Wang, J.F. Zhang, P.F. Feng, P. Guo, Damage formation and suppression in rotary ultrasonic machining of hard and brittle materials: a critical review, Ceram. Int. 44 (2) (2018) 127–1239, https://doi.org/10.1016/j.ceramint.2017.10.050.
[22] M. Arif, M. Rahman, W.Y. San, Analytical model to determine the critical feed per edge for ductile–brittle transition in milling process of brittle materials, Int. J. Mach. Tools Manuf 51 (3) (2011) 170–181, https://doi.org/10.1016/j.ijmachtools.2010.12.003.
[23] J. Zhang, D. Wang, P.F. Feng, Z. Wu, C.L. Zhang, Material removal characteristics of KDP crystal in ultrasonic vibration-assisted scratch process, Mater. Manuf. Processes 31 (8) (2016) 1037–1045, https://doi.org/10.1080/10426914.2015.1070423.
[24] H. Wang, F.D. Ning, Y.B. Hu, Y.C. Li, X.L. Wang, W.L. Cong, Edge trimming of CFRP composites using rotary ultrasonic machining: effects of ultrasonic vibration, ASME 2018 13th International Manufacturing Science and Engineering Conference, American Society of Mechanical Engineers, 2018, , https://doi.org/10.1115/MSEC2018-6362 pp. V004T03A051-V004T03A051.
[25] D. Geng, Y. Liu, Z. Shao, Z. Lu, J. Cai, X. Li, X. Jiang, D. Zhang, Delamination formation, evaluation and suppression during drilling of composite laminates: A review, Compos. Struct. 216 (2019) 168–186, https://doi.org/10.1016/j.compstruct.2019.02.099.
[26] H. Wang, Y.B. Hu, W.L. Cong, Z.L. Hu, A mechanistic model on feeding-directional cutting force in surface grinding of CFRP composites using rotary ultrasonic machining with horizontal ultrasonic vibration, Int. J. Mech. Sci. 155 (2019) 450–460, https://doi.org/10.1016/j.ijmecsci.2019.03.009.
[27] T. Matsumura, T. Hiramatsu, T. Shirakashi, T. Muramatsu, A study on cutting force in the milling process of glass, J. Manuf. Processes 7 (2) (2005) 102–108, https://doi.org/10.1016/S1526-6125(05)70087-6.
[28] Z. Jia, R. Fu, B. Niu, B. Qian, Y. Bai, F. Wang, Novel drill structure for damage reduction in drilling CFRP composites, Int. J. Mach. Tools Manuf 110 (2016) 55–65, https://doi.org/10.1016/j.ijmachtools.2016.08.006.
[29] W. Hintze, D. Hartmann, Modeling of delamination during milling of unidirectional CFRP, Procedia CIRP 8 (2013) 444–449, https://doi.org/10.1016/j.procir.2013.06.131.
[30] Z. Jia, Y. Su, B. Niu, B. Zhang, F. Wang, The interaction between the cutting force and induced sub-surface damage in machining of carbon fiber-reinforced plastics, J. Reinf. Plast. Compos. 35 (9) (2016) 712–726, https://doi.org/10.1177/0731684415626284.